Exchange-Striction Driven Ultrafast Nonthermal Lattice Dynamics in NiO

Y. W. Windsor,[1,*] D. Zahn,[1] R. Kamrla,[2] J. Feldl,[3] H. Seiler,[1] C.-T. Chiang,[2] M. Ramsteiner,[3] W. Widdra,[2] R. Ernstorfer,[1] and L. Rettig[1,†]

[1]*Department of Physical Chemistry, Fritz Haber Institute of the Max Planck Society, Faradayweg 4-6, 14195 Berlin, Germany*
[2]*Institute of Physics, Martin-Luther-Universität Halle-Wittenberg, 06120 Halle, Germany*
[3]*Paul-Drude-Institut für Festkörperelektronik, Leibniz-Institut im Forschungsverbund Berlin e.V., Hausvogteiplatz 5-7, 10117 Berlin, Germany*

(Received 30 October 2020; accepted 3 March 2021; published 8 April 2021)

We use femtosecond electron diffraction to study ultrafast lattice dynamics in the highly correlated antiferromagnetic (AFM) semiconductor NiO. Using the scattering vector (Q) dependence of Bragg diffraction, we introduce Q-resolved effective temperatures describing the transient lattice. We identify a nonthermal lattice state with preferential displacement of O compared to Ni ions, which occurs within ~0.3 ps and persists for 25 ps. We associate this with transient changes to the AFM exchange striction-induced lattice distortion, supported by the observation of a transient Q asymmetry of Friedel pairs. Our observation highlights the role of spin-lattice coupling in routes towards ultrafast control of spin order.

DOI: 10.1103/PhysRevLett.126.147202

NiO has been of interest for several decades, both from fundamental and application perspectives [1–4]. Because of strong correlations, *ab initio* descriptions of this large band gap charge-transfer semiconductor are challenging [5–12]. The open Ni d shell and strong superexchange lead to high-temperature antiferromagnetic (AFM) order ($T_N \approx 523$ K), making NiO a promising candidate for room-temperature spintronic applications [13–15]. In this context, pioneering experiments have demonstrated coherent excitation of high-frequency magnon modes by THz pulses [16–18], fueling the promise of ultrafast AFM spintronics. For such purposes, understanding energy transport due to coupling between the material's subsystems is of importance, in particular those to magnetic order. In equilibrium, NiO exhibits strong spin-lattice coupling and exchange striction [19], leading to a rhombohedral lattice distortion (RLD) along the [111] direction of its nominally cubic structure below T_N [20]. Spin-phonon coupling in NiO has been recently studied in the context of magnon damping in devices [21]. However, energy transfer dynamics and couplings between the various subsystems upon optical excitation have been little studied so far [22]. In particular, to date there is no account of ultrafast lattice dynamics in NiO.

In the presence of a band gap, optically excited carriers can radiatively decay, and they can transfer energy to another subsystem, e.g., the lattice. This is typically described using coupled-heat-baths models [23–25], where the subsystems' transient temperatures are described by coupled rate equations. While often successfully employed [26,27], an implicit assumption is that the baths themselves remain thermalized, such that the carriers and the phonons always follow Fermi-Dirac and Bose-Einstein distributions. Whereas this is considered valid for many metals because of homogenous electron-phonon coupling and rapid electronic thermalization, this assumption has been recently challenged even for simple metallic systems [28–31]. In semiconductors, electron-phonon coupling is often strongly heterogenous [32], and the phonon dispersion is often more complicated than in metals. Consequently, photoexcited semiconductors may experience a prolonged nonthermal lattice state, in which unconventional relaxation processes may occur. To date only a few reports describing nonthermal lattice dynamics of semiconductors have been published [33–37], and details about the underlying microscopic processes are scarce. In complex materials such as NiO, lattice dynamics may be substantially influenced by effects beyond electron-phonon coupling, such as spin-lattice coupling via exchange striction.

Here we use femtosecond electron diffraction (FED) to study photoinduced lattice dynamics in NiO. Variants of FED have recently been used to study lattice dynamics in several other systems, including metals [38,39], semiconductors [34,40], heterostructures [41,42], and systems involving structural phase transitions [43,44]. We present an approach to characterize the transient lattice state, by converting Bragg reflection intensities into units of Kelvin, producing a series of temperatures associated with each scattering vector of the probe electrons (Q). Analysis of

these Q-dependent effective temperatures allows identifying a nonthermal lattice state. Through this we identify a strongly nonthermal lattice state after excitation, which lasts for tens of picoseconds. Employing the Q-dependent Ni^{2+} and O^{2-} scattering factors we gain a varying degree of element sensitivity. Based on its systematic variation with Q, we find that the lattice response to photoexcitation is primarily on oxygen ions, and less on nickel. Based on the initial energy transfer timescale of ~0.3 ps, we propose a scenario in which photoexcitation perturbs the antiferromagnetically induced RLD. This is supported by photoinduced changes in observed Q values that occur due to changes in the shape of the unit cell (i.e., the RLD), suggesting that the observed nonthermal lattice state originates from preferential occupation of phonon modes associated with the RLD.

We use a 20 nm thick single crystal of NiO, epitaxially grown on a [001]-oriented NaCl crystal, which was subsequently dissolved. Diffraction and Raman measurements confirmed its bulklike properties (see Supplemental Material [45]). Experiments were conducted at room temperature (T_0) using a compact setup [46] [Fig. 1(a)], with femtosecond laser excitation of $h\nu = 2.16$ eV and 5.2 ± 1.3 mJ cm^{-2} incident fluence. This photon energy slightly exceeds half the charge-transfer gap of $\Delta \approx 3.8$ eV [22,47,48], and two-photon absorption is likely dominant over linear absorption (see Supplemental Material [45] for details, including Refs. [49–52]). 70 keV probe electrons transmit through the sample, producing patterns as in Fig. 1(b). The response function is estimated at 200 fs.

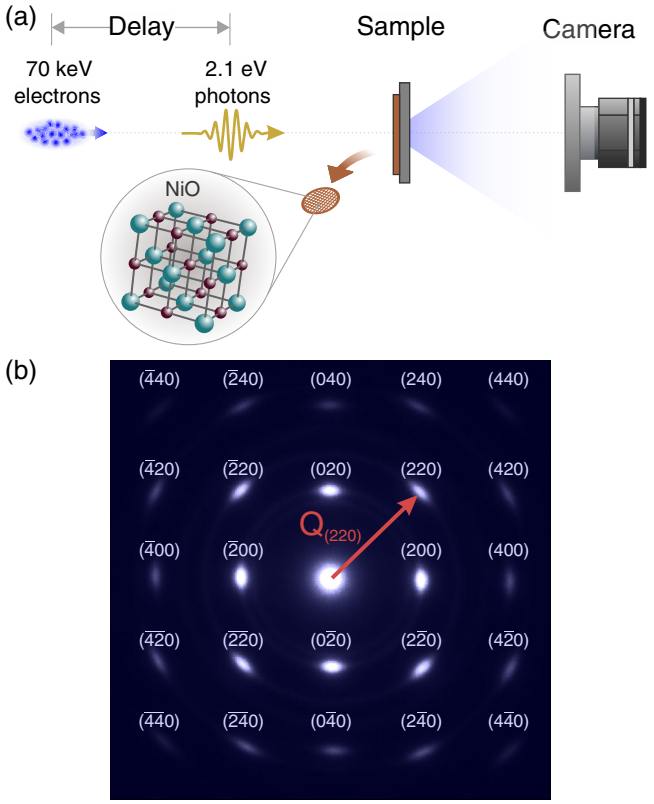

FIG. 1. (a) Experimental scheme. (b) Example diffraction pattern. Arrow: exemplary scattering vector. In this work "Q" denotes the length of this vector.

The lattice response was measured using diffraction patterns from different pump-probe delays t. The observed diffraction spots correspond to reflections with Miller indices ($hk0$). Faint rings are also observed, all corresponding to NiO Bragg reflections, likely from polycrystalline regions. Intensities of > 50 diffraction spots were extracted, covering 10 values of Q [defined as $Q = 2\lambda^{-1}\sin\theta$; λ and θ are electron wavelength and Bragg angle; see Fig. 1(b)]. Intensities from spots of equal Q were averaged, producing 10 independent intensity observables $I_Q(t)$, shown in Fig. 2(a). All $I_Q(t)$ curves exhibit an initial sub-picosecond drop, followed by a slower process.

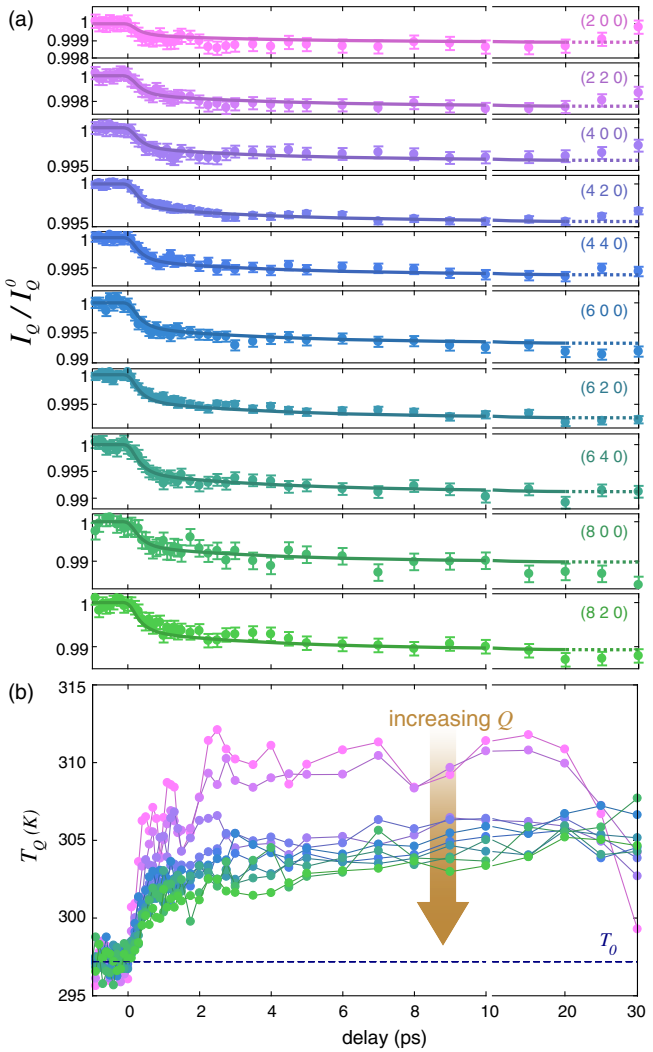

FIG. 2. (a) Normalized transient Bragg intensities: each I_Q curve represents the mean response of all Bragg reflections with the same scattering vector length Q. Labels: representative ($hk0$) indices. Lines are calculated from the $\bar{T}$ fit [Fig. 4(b)] using Eq. (1). I_Q^0 is the unpumped I_Q. (b) Q-dependent effective temperatures T_Q. Each curve is calculated from Fig. 2(a) using tabulated temperature-dependent DW factors in Eq. (1).

We describe Bragg intensities using structure factor calculations. Intensities of ($hk0$) reflections depend only on the size of Q [53].

$$I_Q \propto |f_{\mathrm{Ni}}(Q)e^{-Q^2B_{\mathrm{Ni}}} + f_O(Q)e^{-Q^2B_O}|^2. \quad (1)$$

Here f_{Ni} and f_O are the scattering factors of the Ni^{2+} and O^{2-} ions, which are tabulated functions of Q (see discussion in Supplemental Material [45], including Refs. [54–59]). B_{Ni} and B_O are the Debye-Waller (DW) factors for Ni and O ions, which are tabulated as functions of temperature for NiO [59]. DW factors can be expressed as $B_x = \frac{2}{3}\pi^2\langle u_x^2\rangle$ (x represents Ni or O), in which $\langle u_x^2\rangle$ are the time-averaged mean square displacement (MSD) of the Ni^{2+} or O^{2-} ions, i.e., a measure of each atom species' vibrations $u_x(t)$ about their mean position. Upon heating in equilibrium conditions, the MSDs and thereby the DW factors increase due to the growing phonon population, causing a reduction in diffracted intensity (DW effect). Similarly, MSDs can also increase upon photoexcitation if a phonon population is induced, and serve as reliable measures for the lattice response to laser excitation [40].

Since B_{Ni} and B_O in Eq. (1) cannot be analytically separated (see Supplemental Material [45]), we adopt a temperature-based approach. We insert the tabulated $B_{\mathrm{Ni}}(T)$ and $B_O(T)$ into Eq. (1) to convert the relative intensities $I_Q(t)$ into temperatures $T_Q(t)$, in units of Kelvin. The T_Q curves, shown in Fig. 2(b), represent *effective* temperatures describing the transient lattice state, because our conversion is based on equilibrium (i.e., *thermal*) DW factors, while the phonon population may be *nonthermal* after photoexcitation. Nevertheless, the $T_Q(t)$ curves provide a Q-resolved picture that can now be used to describe the nonthermal state of the lattice.

The T_Q curves in Fig. 2(b) deviate significantly from each other, both in the rise magnitude (higher temperatures observed towards lower Q) and in their qualitative behavior. To explain this, we consider that different Q provide varying sensitivity to the Ni^{2+} and O^{2-} ions through the Q dependence of their respective scattering factors f_{Ni} and f_O in Eq. (1). Figure 3(a) presents their squared ratio $\eta(Q) = (f_{\mathrm{Ni}}/f_O)^2$, reflecting the relative element sensitivity in the diffracted intensity [i.e., in the squared structure factor of Eq. (1)], in a range covering all probed Q values. Because of the large difference between scattering from Ni^{2+} and from O^{2-}, η shows a significant and continuous variation in this range, demonstrating that Bragg reflections at higher Q values are more sensitive to scattering from Ni^{2+} than from O^{2-}.

To demonstrate this, Fig. 3(b) presents T_Q as a function of Q at selected delays. Before excitation T_Q exhibits no Q dependence, as expected in a thermal state (all $T_Q = T_0$). After excitation, T_Q exhibits an overall increase in temperature due to the excitation, with a *continuous* reduction upon increasing Q. This marks a departure from equilibrium

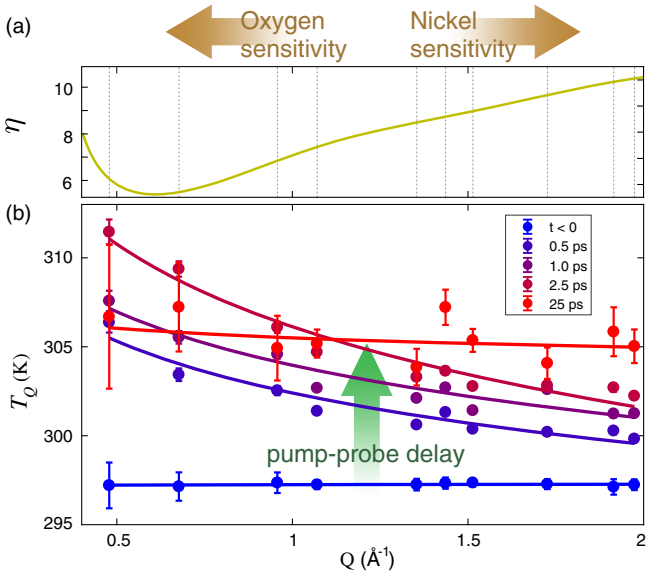

FIG. 3. (a) Calculated squared ratio between Ni^{2+} and O^{2-} scattering factors $\eta(Q) = (f_{\mathrm{Ni}}/f_O)^2$ as a function of scattering vector length Q. Dashed lines mark discreet Q values probed in the experiment. (b) Q-dependent lattice temperatures T_Q at selected delays. Solid lines are fits to $T_Q \propto Q^b$. This neglects $\eta's$ minimum, as it is obscured by larger uncertainties at low Q.

behavior. Combined with the continuous growth in sensitivity to oxygen vibrations with decreasing Q [Fig. 3(a)], this result indicates that the MSD of oxygen $\langle u_O^2\rangle$ initially grows *disproportionately* more than that of nickel $\langle u_{\mathrm{Ni}}^2\rangle$, demonstrating a nonthermal lattice state at early times. This trend is subsequently suppressed, such that at 25 ps the Q dependence of T_Q is nearly flat, indicating thermalization of the lattice. This disproportionate growth is not to be confused with the *absolute* difference between O and Ni MSDs, which differ also in equilibrium [58].

We quantify this nonthermal disproportionality between the O and Ni vibrational responses by empirically describing these Q dependences as $T_Q \propto Q^b$ [solid lines, Fig. 3(b)]. Figure 4(a) presents $b(t)$ at each delay, exhibiting an initial sub-ps reduction, and reaching a minimum at 3 ps, corresponding to the most pronounced disproportionality between O and Ni. After ~15 ps, $b(t)$ recovers toward 0, i.e., to a thermal lattice state, which is also reflected in the difference between the T_Q curves in Fig. 2(b).

$\eta(Q)$ also enables a reliable description of the *mean* lattice response. Averaging η-weighted T_Q data [Fig. 2(b)] produces a mean lattice response $\bar{T}(t)$, presented in Fig. 4(b). As in $I_Q(t)$, $\bar{T}(t)$ exhibits a two-step response, well described by a biexponential. The best fit (solid line) yields a sub-ps process ($\tau_1 = 0.31 \pm 0.08$ ps) and a second, slower one ($\tau_2 = 4.1 \pm 1.3$ ps), see dashed lines. The total temperature rise is $\Delta T = 9.6 \pm 0.7$ K, of which 60% is the fast process. Using the NiO lattice heat capacity [61], we find that ΔT corresponds to a maximal change of

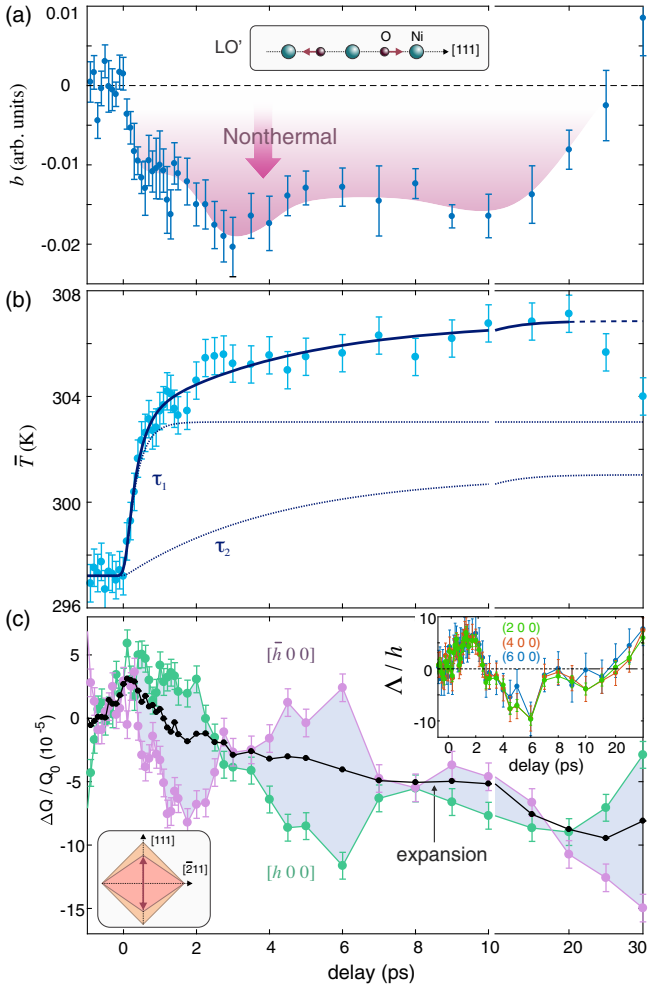

FIG. 4. (a) The coefficient $b(t)$, describing transient changes in the Q dependence of T_Q [as in Fig. 3(b)]. The dashed line indicates zero (thermal lattice state). Inset: Schematic of the LO' motions (arrows) [21]. (b) η-weighted mean lattice temperature. The solid line is the best fit to a biexponential (convolved with Gaussian instrument response). Dashed lines represent the two individual processes. (c) Relative change in peak positions. Black: average of all ($hk0$) reflections. The feature near time zero is likely caused by space-charge interactions [60]. Green/purple: evolution of Q along two opposite directions: [h 0 0] and [$\bar{h}$ 0 0] (averaged over $h = 2, 4, 6$). Insets: Top: Asymmetry Λ for [h00] [in units of (detector pixels)^2], normalized by h. Bottom: sketch of the rhombohedral distortion of the cubic unit cell.

16 ± 1 meV/unit cell in the lattice energy density. Careful evaluation of the data concluded that the fast process is intrinsic, while the slower process evolves as the measurement progresses (see Supplemental Material [45]). Late delays were omitted from the fit because they exhibit recovery, similar to that of $b(t)$ [Fig. 4(a)]. We convert $\bar{T}(t)$ back into Bragg intensities by η weighing the $\bar{T}(t)$ fit and plugging it into Eq. (1). This produces the lines in Fig. 2(a), in reasonably good agreement with the data. Disagreements exist because this washes out the distinctly nonthermal description in Fig. 4(a). Our fit does not consider recovery, so at late delays the Q dependence of η causes I_Q data with low (high) Q to be above (below) the lines.

To interpret the stronger response of the O ions, we inspect the phonon dispersion of NiO. Already in the unperturbed NaCl structure this reveals several optical phonons that preferentially move the O ions, such as at the L and W points (Brillouin zone boundary along [111] and [110]). Below T_N, the optical modes' frequencies deviate significantly from the expected temperature dependence of crystal lattice anharmonicity [21], and they split in energy [62] due to the RLD [63,64], creating modes such as the LO' mode, which displaces only O ions [21]. Preferential coupling to such modes would lead to their enhanced population in a nonthermal phonon distribution, followed by thermalization of the excited phonon population to lower energy/momentum modes, on phonon-phonon scattering timescales [32,65]. A scenario leading to a preferential excitation of such modes could be a perturbation of the AFM-induced RLD, for which a full crystallographic account was only recently reported [66]. Following Uchiyama [64], two effects contribute to this distortion, which acts along [111] [sketched in Fig. 4(c)]. The first is a distortion caused directly by the nearest-neighbor superexchange [67]. The second originates from Coulomb forces induced by an asymmetric charge distribution around the ions, due to AFM-induced band folding [63,64], predicted to be the dominant contribution [64].

This suggests two possibilities for perturbing the distortion. The first is that the excitation weakens the AFM order, and therefore also the charge asymmetry, both of which then weaken the distortion. The lattice response time ($\tau_1 \approx 0.31$ ps) should then reflect magnetic excitation times. Reported optically excited magnon data indeed suggest similar timescales [68–70]. However, a magnetic diffraction experiment has disputed these results [71]. The second possibility is that the charge asymmetry is directly perturbed, without involving magnetism. An excitation above the gap could cause a displacive phonon excitation. However, timescales associated with electronic excitations in NiO are much shorter than τ_1 [72], and displacive phonon excitations in similar binary oxides occur on much shorter timescales [73,74], so we conclude that this possibility is unlikely.

This brings about the following scenario. Electrons are optically excited above the gap and magnetic order rapidly weakens. This reduces the asymmetric charge distribution, triggering lattice motions that weaken the RLD. Because of this preferential electron-phonon coupling, modes that lead to a reduction of the RLD are preferentially occupied, which is observed as disproportionally higher growth of $\langle u_O^2 \rangle$. The lattice subsequently reaches an elevated thermal state via phonon-phonon coupling within ~25 ps. This scenario should directly affect other observables, such as the phononic energy gap or the rhombohedral angle itself. Additional phonon-phonon relaxation

processes are likely to occur concomitantly, as expected in semiconductors [32].

To support this scenario, we consider how varying the RLD would affect the observed scattering vectors, i.e., the *positions* of the spots [Fig. 1(b)]. We divide them into Friedel pairs of the form $(hk0)$ and $(\bar{h}\,\bar{k}\,0)$, and extract the change in peak position $\Delta Q(t) = Q(t) - Q_0$ for each spot individually, as well as the average ΔQ of each pair. The average ΔQ curves of all pairs closely reproduce each other [black symbols in Fig. 4(c)], and exhibit a slow decrease of Q indicating isotropic lattice expansion (i.e., $a = b$ at all delays). Combining ΔQ with ΔT [Fig. 4(b)] produces an expansion coefficient of $\sim 10^{-5}$ K^{-1}, in agreement with literature [75]. However, the individual spots in every pair deviate symmetrically around this mean [shown for the $(h00)$ family in Fig. 4(c)]. To quantify this, we introduce the asymmetry $\Lambda = Q^2(hk0) - Q^2(\bar{h}\,\bar{k}\,0)$ (accounting for Ewald's sphere curvature, see Supplemental Material [45]). A nonzero Λ represents deviations from an orthonormal unit cell, and scales as $\Lambda \propto (h + k)$ (see Supplemental Material [45]). The inset presents $\Lambda(t)$ calculated from the same data as Fig. 4(c), exhibiting this scaling. While $\Lambda(t)$ does not immediately translate into the magnitude of the RLD, its nontrivial dynamics demonstrate transient changes in it. Therefore, these data serve as direct evidence of a transient change in the *shape* of the unit cell upon excitation, supporting the scenario of pump-induced changes in the RLD [lower inset, Fig. 4(c)]. They underline the role of spin-lattice coupling through exchange striction in the ultrafast lattice dynamics of NiO. Ultimately, this efficient spin-lattice coupling may facilitate ultrafast spintronic applications, e.g., by enabling structural control of magnetism.

In summary, we studied the lattice response of NiO to photoexcitation using femtosecond electron diffraction. Describing the data as scattering-vector-dependent effective temperatures enabled us to study the transient nonthermal state of the lattice. Compared to thermal conditions, this state involves a disproportionally higher displacement of O ions compared to Ni. While the lattice response time is ~0.31 ps, the nonthermal state persists for up to ~25 ps, after which the system reaches a new thermal state. We present a scenario in which this nonthermal state is facilitated by perturbation of the antiferromagnetically induced rhombohedral lattice distortion. This is supported by observed changes in the asymmetry of Bragg peak positions of Friedel pairs, a hallmark of nonorthonormal systems. Our results shed light on the nature of the nonthermal lattice state in NiO, and demonstrate how spin-lattice coupling through exchange striction may play a key role in future ultrafast applications.

The data used herein are available online [76].

This work received funding from the DFG within the Emmy Noether program under Grant No. RE 3977/1, and within the Transregio TRR 227 Ultrafast Spin Dynamics (Projects No. A09, No. B07 and No. A06). Funding was also received from the Max Planck Society, and from the European Research Council (ERC) under the European Union's Horizon 2020 research and innovation program (Grant Agreement No. ERC-2015-CoG-682843). H. S. acknowledges support by the Swiss National Science Foundation under Grant No. P2SKP2.184100.

*windsor@fhi-berlin.mpg.de
†rettig@fhi-berlin.mpg.de

[1] U. Kaiser, A. Schwarz, and R. Wiesendanger, Magnetic exchange force microscopy with atomic resolution, Nature (London) **446**, 522 (2007).
[2] J. You, L. Meng, T.-B. Song, T.-F. Guo, Y. (Michael) Yang, W.-H. Chang, Z. Hong, H. Chen, H. Zhou, Q. Chen, Y. Liu, N. De Marco, and Y. Yang, Improved air stability of perovskite solar cells via solution-processed metal oxide transport layers, Nat. Nanotechnol. **11**, 75 (2016).
[3] M. Gong, W. Zhou, M.-C. Tsai, J. Zhou, M. Guan, M.-C. Lin, B. Zhang, Y. Hu, D.-Y. Wang, J. Yang, S. J. Pennycook, B.-J. Hwang, and H. Dai, Nanoscale nickel oxide/nickel heterostructures for active hydrogen evolution electrocatalysis, Nat. Commun. **5**, 4695 (2014).
[4] J. Feldl, M. Budde, C. Tschammer, O. Bierwagen, and M. Ramsteiner, Magnetic characteristics of epitaxial NiO films studied by Raman spectroscopy, J. Appl. Phys. **127**, 235105 (2020).
[5] K. Terakura, A. R. Williams, T. Oguchi, and J. Kübler, Transition-Metal Monoxides: Band or Mott Insulators, Phys. Rev. Lett. **52**, 1830 (1984).
[6] Z.-X. Shen, R. S. List, D. S. Dessau, B. O. Wells, O. Jepsen, A. J. Arko, R. Barttlet, C. K. Shih, F. Parmigiani, J. C. Huang, and P. A. P. Lindberg, Electronic structure of NiO: Correlation and band effects, Phys. Rev. B **44**, 3604 (1991).
[7] F. Aryasetiawan and O. Gunnarsson, Electronic Structure of NiO in the *GW* Approximation, Phys. Rev. Lett. **74**, 3221 (1995).
[8] T. Archer, C. D. Pemmaraju, S. Sanvito, C. Franchini, J. He, A. Filippetti, P. Delugas, D. Puggioni, V. Fiorentini, R. Tiwari, and P. Majumdar, Exchange interactions and magnetic phases of transition metal oxides: Benchmarking advanced ab initio methods, Phys. Rev. B **84**, 115114 (2011).
[9] C. Mitra, J. T. Krogel, J. A. Santana, and F. A. Reboredo, Many-body ab initio diffusion quantum Monte Carlo applied to the strongly correlated oxide NiO, J. Chem. Phys. **143**, 164710 (2015).
[10] G. Trimarchi, Z. Wang, and A. Zunger, Polymorphous band structure model of gapping in the antiferromagnetic and paramagnetic phases of the Mott insulators MnO, FeO, CoO, and NiO, Phys. Rev. B **97**, 035107 (2018).
[11] Y. Gao, Q. Sun, J. M. Yu, M. Motta, J. McClain, A. F. White, A. J. Minnich, and Garnet Kin-Lic Chan, Electronic structure of bulk manganese oxide and nickel oxide from coupled cluster theory, Phys. Rev. B **101**, 165138 (2020).

[12] J. Kuneš, V. I. Anisimov, A. V Lukoyanov, and D. Vollhardt, Local correlations and hole doping in NiO: A dynamical mean-field study, Phys. Rev. B **75**, 165115 (2007).
[13] I. Sugiyama, N. Shibata, Z. Wang, S. Kobayashi, T. Yamamoto, and Y. Ikuhara, Ferromagnetic dislocations in antiferromagnetic NiO, Nat. Nanotechnol. **8**, 266 (2013).
[14] W. Lin, K. Chen, S. Zhang, and C. L. Chien, Enhancement of Thermally Injected Spin Current through an Antiferromagnetic Insulator, Phys. Rev. Lett. **116**, 186601 (2016).
[15] F. L. A. Machado, P. R. T. Ribeiro, J. Holanda, R. L. Rodríguez-Suárez, A. Azevedo, and S. M. Rezende, Spin-flop transition in the easy-plane antiferromagnet nickel oxide, Phys. Rev. B **95**, 104418 (2017).
[16] T. Kampfrath, A. Sell, G. Klatt, A. Pashkin, S. Mährlein, T. Dekorsy, M. Wolf, M. Fiebig, A. Leitenstorfer, and R. Huber, Coherent terahertz control of antiferromagnetic spin waves, Nat. Photonics **5**, 31 (2011).
[17] S. Baierl, J. H. Mentink, M. Hohenleutner, L. Braun, T.-M. Do, C. Lange, A. Sell, M. Fiebig, G. Woltersdorf, T. Kampfrath, and R. Huber, Terahertz-Driven Nonlinear Spin Response of Antiferromagnetic Nickel Oxide, Phys. Rev. Lett. **117**, 197201 (2016).
[18] Z. Wang, S. Kovalev, N. Awari, M. Chen, S. Germanskiy, B. Green, J.-C. Deinert, T. Kampfrath, J. Milano, and M. Gensch, Magnetic field dependence of antiferromagnetic resonance in NiO, Appl. Phys. Lett. **112**, 252404 (2018).
[19] H. P. Rooksby, A note on the structure of nickel oxide at subnormal and elevated temperatures, Acta Crystallogr. **1**, 226 (1948).
[20] L. C. Bartel and B. Morosin, Exchange striction in NiO, Phys. Rev. B **3**, 1039 (1971).
[21] E. Aytan, B. Debnath, F. Kargar, Y. Barlas, M. M. Lacerda, J. X. Li, R. K. Lake, J. Shi, and A. A. Balandin, Spin-phonon coupling in antiferromagnetic nickel oxide, Appl. Phys. Lett. **111**, 252402 (2017).
[22] K. Gillmeister, D. Golež, C.-T. Chiang, N. Bittner, Y. Pavlyukh, J. Berakdar, P. Werner, and W. Widdra, Ultrafast coupled charge and spin dynamics in strongly correlated NiO, Nat. Commun. **11**, 4095 (2020).
[23] M. I. Kaganov, I. M. Lifshitz, and L. V. Tanatarov, Relaxation between electrons and the Crystalline Lattice, Sov. Phys. JETP **31**, 173 (1957), http://www.jetp.ac.ru/cgi-bin/e/index/e/4/2/p173?a=list.
[24] P. B. Allen, Theory of Thermal Relaxation of Electrons in Metals, Phys. Rev. Lett. **59**, 1460 (1987).
[25] E. Beaurepaire, J.-C. Merle, A. Daunois, and J.-Y. Bigot, Ultrafast Spin Dynamics in Ferromagnetic Nickel, Phys. Rev. Lett. **76**, 4250 (1996).
[26] H. E. Elsayed-Ali, T. B. Norris, M. A. Pessot, and G. A. Mourou, Time-Resolved Observation of Electron-Phonon Relaxation in Copper, Phys. Rev. Lett. **58**, 1212 (1987).
[27] A. Nakamura, T. Shimojima, M. Nakano, Y. Iwasa, and K. Ishizaka, Electron and lattice dynamics of transition metal thin films observed by ultrafast electron diffraction and transient optical measurements, Struct. Dyn. **3**, 064501 (2016).
[28] L. Waldecker, R. Bertoni, R. Ernstorfer, and J. Vorberger, Electron-Phonon Coupling and Energy Flow in a Simple Metal beyond the Two-Temperature Approximation, Phys. Rev. X **6**, 021003 (2016).
[29] J.-A. Yang, S. Parham, D. Dessau, and D. Reznik, Novel electron-phonon relaxation pathway in graphite revealed by time-resolved raman scattering and angle-resolved photoemission spectroscopy, Sci. Rep. **7**, 40876 (2017).
[30] M. J. Stern, L. P. Rene de Cotret, M. R. Otto, R. P. Chatelain, J.-P. Boisvert, M. Sutton, and B. J. Siwick, Mapping momentum-dependent electron-phonon coupling and nonequilibrium phonon dynamics with ultrafast electron diffuse scattering, Phys. Rev. B **97**, 165416 (2018).
[31] R. P. Chatelain, V. R. Morrison, B. L. M. Klarenaar, and B. J. Siwick, Coherent and Incoherent Electron-Phonon Coupling in Graphite Observed with Radio-Frequency Compressed Ultrafast Electron Diffraction, Phys. Rev. Lett. **113**, 235502 (2014).
[32] S. Sadasivam, M. K. Y. Chan, and P. Darancet, Theory of Thermal Relaxation of Electrons in Semiconductors, Phys. Rev. Lett. **119**, 136602 (2017).
[33] D. Zahn, P.-N. Hildebrandt, T. Vasileiadis, Y. W. Windsor, Y. Qi, H. Seiler, and R. Ernstorfer, Anisotropic nonequilibrium lattice dynamics of black phosphorus, Nano Lett. **20**, 3728 (2020).
[34] L. Waldecker, R. Bertoni, H. Hübener, T. Brumme, T. Vasileiadis, D. Zahn, A. Rubio, and R. Ernstorfer, Momentum-Resolved View of Electron-Phonon Coupling in Multilayer WSe_2, Phys. Rev. Lett. **119**, 036803 (2017).
[35] M. Trigo, J. Chen, V. H. Vishwanath, Y. M. Sheu, T. Graber, R. Henning, and D. A. Reis, Imaging nonequilibrium atomic vibrations with x-ray diffuse scattering, Phys. Rev. B **82**, 235205 (2010).
[36] M. Trigo, M. Fuchs, J. Chen, M. P. Jiang, M. Cammarata, S. Fahy, D. M. Fritz, K. Gaffney, S. Ghimire, A. Higginbotham, S. L. Johnson, M. E. Kozina, J. Larsson, H. Lemke, A. M. Lindenberg, G. Ndabashimiye, F. Quirin, K. Sokolowski-Tinten, C. Uher, G. Wang, J. S. Wark, D. Zhu, and D. A. Reis, Fourier-transform inelastic X-ray scattering from time- and momentum-dependent phonon–phonon correlations, Nat. Phys. **9**, 790 (2013).
[37] T. Henighan, M. Trigo, M. Chollet, J. N. Clark, S. Fahy, J. M. Glownia, M. P. Jiang, M. Kozina, H. Liu, S. Song, D. Zhu, and D. A. Reis, Control of two-phonon correlations and the mechanism of high-wavevector phonon generation by ultrafast light pulses, Phys. Rev. B **94**, 020302(R) (2016).
[38] R. Ernstorfer, M. Harb, C. T. Hebeisen, G. Sciaini, T. Dartigalongue, and R. J. D. Miller, The formation of warm dense matter: Experimental evidence for electronic bond hardening in gold, Science **323**, 1033 (2009).
[39] L. Waldecker, T. Vasileiadis, R. Bertoni, R. Ernstorfer, T. Zier, F. H. Valencia, M. E. Garcia, and E. S. Zijlstra, Coherent and incoherent structural dynamics in laser-excited antimony, Phys. Rev. B **95**, 054302 (2017).
[40] V. Tinnemann, C. Streubühr, B. Hafke, A. Kalus, A. Hanisch-Blicharski, M. Ligges, P. Zhou, D. von der Linde, U. Bovensiepen, and M. Horn-von Hoegen, Ultrafast electron diffraction from a Bi(111) surface: Impulsive lattice excitation and Debye–Waller analysis at large momentum transfer, Struct. Dyn. **6**, 035101 (2019).
[41] K. Sokolowski-Tinten, X. Shen, Q. Zheng, T. Chase, R. Coffee, M. Jerman, R. K. Li, M. Ligges, I. Makasyuk, M. Mo, A. H. Reid, B. Rethfeld, T. Vecchione, S. P. Weathersby, H. A. Dürr, and X. J. Wang, Electron-lattice energy relaxation

in laser-excited thin-film Au-insulator heterostructures studied by ultrafast MeV electron diffraction, Struct. Dyn. **4**, 054501 (2017).

[42] T. Vasileiadis, E. N. Skountzos, D. Foster, S. P. Coleman, D. Zahn, F. Krečinić, V. G. Mavrantzas, R. E. Palmer, and R. Ernstorfer, Ultrafast rotational motions of supported nanoclusters probed by electron diffraction, Nanoscale Horiz. **4**, 1164 (2019).

[43] T. Frigge, B. Hafke, T. Witte, B. Krenzer, C. Streubühr, A. Samad Syed, V. Mikšić Trontl, I. Avigo, P. Zhou, M. Ligges, D. Von Der Linde, U. Bovensiepen, M. Horn-Von Hoegen, S. Wippermann, A. Lücke, S. Sanna, U. Gerstmann, and W. G. Schmidt, Optically excited structural transition in atomic wires on surfaces at the quantum limit, Nature (London) **544**, 207 (2017).

[44] A. Kogar, A. Zong, P. E. Dolgirev, X. Shen, J. Straquadine, Y. Q. Bie, X. Wang, T. Rohwer, I. C. Tung, Y. Yang, R. Li, J. Yang, S. Weathersby, S. Park, M. E. Kozina, E. J. Sie, H. Wen, P. Jarillo-Herrero, I. R. Fisher, X. Wang, and N. Gedik, Light-induced charge density wave in $LaTe_3$, Nat. Phys. **16**, 159 (2020).

[45] See Supplemental Material at http://link.aps.org/supplemental/10.1103/PhysRevLett.126.147202 for sample growth and characterization, as well as further experimental and data analysis details.

[46] L. Waldecker, R. Bertoni, and R. Ernstorfer, Compact femtosecond electron diffractometer with 100 keV electron bunches approaching the single-electron pulse duration limit, J. Appl. Phys. **117**, 044903 (2015).

[47] G. A. Sawatzky and J. W. Allen, Magnitude and Origin of the Band Gap in NiO, Phys. Rev. Lett. **53**, 2339 (1984).

[48] F. Reinert and S. Hüfner, Photoemission spectroscopy—from early days to recent applications, New J. Phys. **7**, 97 (2005).

[49] M. Harb, R. Ernstorfer, T. Dartigalongue, C. T. Hebeisen, R. E. Jordan, and R. J. D. Miller, Carrier relaxation and lattice heating dynamics in silicon revealed by femtosecond electron diffraction, J. Phys. Chem. B **110**, 25308 (2006).

[50] R. Newman and R. M. Chrenko, Optical properties of nickel oxide, Phys. Rev. **114**, 1507 (1959).

[51] S. P. Zeuschner, J.-E. Pudell, A. von Reppert, M. Deb, E. Popova, N. Keller, M. Rössle, M. Herzog, and M. Bargheer, Measurement of transient strain induced by two-photon excitation, Phys. Rev. Research **2**, 022013 (2020).

[52] S. I. Shablaev and R. V. Pisarev, Giant nonlinear absorption in the NiO antiferromagnet, Phys. Solid State **45**, 1742 (2003).

[53] The rhombohedral distortion away from 90° reaches ~0.06° at room temperature, so the NaCl-type cubic structure is commonly assumed.

[54] L.-M. Peng, S. L. Dudarev, and M. J. Whelan, Ionicity of nickel oxide: Direct determination by reflection diffraction of high-energy electrons from the (100) surface, Phys. Rev. B **56**, 15314 (1997).

[55] N. F. Mott and W. L. Bragg, The scattering of electrons by atoms, Proc. R. Soc. A **127**, 658 (1930).

[56] L. M. Peng, Electron atomic scattering factors and scattering potentials of crystals, Micron **30**, 625 (1999).

[57] H. Bethe, Zur theorie des durchgangs schneller korpuskularstrahlen durch materie, Ann. Phys. (Berlin) **397**, 325 (1930).

[58] H. X. Gao, L.-M. Peng, and J. M. Zuo, Lattice dynamics and Debye-Waller factors of some compounds with the sodium chloride structure, Acta Crystallogr. Sect. A **55**, 1014 (1999).

[59] L. M. Peng, S. L. Dudarev, and M. J. Whelan, *High-Energy Electron Diffraction and Microscopy* (Oxford University Press, Oxford, 2004).

[60] C. T. Hebeisen, G. Sciaini, M. Harb, R. Ernstorfer, S. G. Kruglik, and R. J. Dwayne Miller, Direct visualization of charge distributions during femtosecond laser ablation of a Si (100) surface, Phys. Rev. B **78**, 081403(R) (2008).

[61] R. A. Coy, C. W. Tompson, and E. Gürmen, Phonon dispersion in NiO, Solid State Commun. **18**, 845 (1976).

[62] C. Kant, F. Mayr, T. Rudolf, M. Schmidt, F. Schrettle, J. Deisenhofer, and A. Loidl, Spin-phonon coupling in highly correlated transition-metal monoxides, Eur. Phys. J. Special Topics **180**, 43 (2009).

[63] H. Uchiyama, S. Tsutsui, and A. Q. R. Baron, Effects of anisotropic charge on transverse optical phonons in NiO: Inelastic x-ray scattering spectroscopy study, Phys. Rev. B **81**, 241103(R) (2010).

[64] H. Uchiyama, Potential asymmetry in antiferromagnetic 3*d* transition metal monoxides, Phys. Rev. B **85**, 014419 (2012).

[65] S. W. Teitelbaum, T. Henighan, Y. Huang, H. Liu, M. P. Jiang, D. Zhu, M. Chollet, T. Sato, É. D. Murray, S. Fahy, S. O'Mahony, T. P. Bailey, C. Uher, M. Trigo, and D. A. Reis, Direct Measurement of Anharmonic Decay Channels of a Coherent Phonon, Phys. Rev. Lett. **121**, 125901 (2018).

[66] D. Rodic, V. Spasojevic, V. Kusigerski, R. Tellgren, and H. Rundlof, Magnetic Ordering in Polycrystalline NixZn1—xO Solid Solutions, Phys. Status Solidi Basic Res. **218**, 527 (2000).

[67] W. Luo, P. Zhang, and M. L. Cohen, Splitting of the zone-center phonon in MnO and NiO, Solid State Commun. **142**, 504 (2007).

[68] C. Tzschaschel, K. Otani, R. Iida, T. Shimura, H. Ueda, S. Günther, M. Fiebig, and T. Satoh, Ultrafast optical excitation of coherent magnons in antiferromagnetic NiO, Phys. Rev. B **95**, 174407 (2017).

[69] T. Satoh, S.-J. Cho, R. Iida, T. Shimura, K. Kuroda, H. Ueda, Y. Ueda, B. A. Ivanov, F. Nori, and M. Fiebig, Spin Oscillations in Antiferromagnetic NiO Triggered by Circularly Polarized Light, Phys. Rev. Lett. **105**, 077402 (2010).

[70] M. Takahara, H. Jinn, S. Wakabayashi, T. Moriyasu, and T. Kohmoto, Observation of coherent acoustic phonons and magnons in an antiferromagnet NiO, Phys. Rev. B **86**, 094301 (2012).

[71] L. Huber, A. Ferrer, T. Kubacka, T. Huber, C. Dornes, T. Sato, K. Ogawa, K. Tono, T. Katayama, Y. Inubushi, M. Yabashi, Y. Tanaka, P. Beaud, M. Fiebig, V. Scagnoli, U. Staub, and S. L. Johnson, Coherent acoustic perturbation of second-harmonic generation in NiO, Phys. Rev. B **92**, 094304 (2015).

[72] K. Gillmeister, M. Kiel, and W. Widdra, Image potential states at transition metal oxide surfaces: A time-resolved two-photon photoemission study on ultrathin NiO films, Phys. Rev. B **97**, 085424 (2018).

[73] E. M. Bothschafter, A. Paarmann, E. S. Zijlstra, N. Karpowicz, M. E. Garcia, R. Kienberger, and R. Ernstorfer, Ultrafast Evolution of the Excited-State Potential Energy Surface of TiO_2 Single Crystals Induced by Carrier Cooling, Phys. Rev. Lett. **110**, 067402 (2013).

[74] H. J. Zeiger, J. Vidal, T. K. Cheng, E. P. Ippen, G. Dresselhaus, and M. S. Dresselhaus, Theory for displacive excitation of coherent phonons, Phys. Rev. B **45**, 768 (1992).

[75] J. E. Keem and J. M. Honig, *Selected Electrical and Thermal Properties of Undoped Nickel Oxide* (Defense Technical Information Center, 1978), https://apps.dtic.mil/sti/citations/ADA128940.

[76] Y. W. Windsor, D. Zahn, R. Kamrla, J. Feldl, H. Seiler, C.-T. Chiang, M. Ramsteiner, W. Widdra, R. Ernstorfer, and L. Rettig, Zenodo (2021), https://doi.org/10.5281/zenodo.4581437.